Published in final edited form as:

Ann Vasc Surg. 2017 May ; 41: 225–234. doi:10.1016/j.avsg.2016.09.014.

Increased oxidative stress and hypoxia inducible factor-1 expression during arteriovenous fistula maturation

Nirvana Sadaghianloo[1,2,§], **Kota Yamamoto**[1,3,4], **Hualong Bai**[1,5], **Masayuki Tsuneki**[6,7], **Clinton D Protack**[1,3], **Michael R Hall**[1,3], **Serge Declemy**[2], **Réda Hassen-Khodja**[2], **Joseph Madri**[7], and **Alan Dardik**[1,3,8]

[1]Vascular Biology and Therapeutics Program, Yale University School of Medicine, New Haven, CT, USA

[2]Department of Vascular Surgery, University Hospital of Nice – Sophia Antipolis, Nice, France

[3]Department of Surgery, Yale University School of Medicine, New Haven, CT, USA

[4]Division of Vascular Surgery, Department of Surgery, Graduate School of Medicine, The University of Tokyo, Tokyo, Japan

[5]Department of Vascular Surgery, First Affiliated Hospital of Zhengzhou University, Henan, China

[6]National Cancer Center Research Institute, Tokyo, Japan

[7]Department of Pathology, Yale University School of Medicine, New Haven, CT, USA

[8]Veterans Affairs Connecticut Healthcare Systems, West Haven, CT, USA

Abstract

Background—The poor clinical results that are frequently reported for arteriovenous fistulae (AVF) for hemodialysis are typically due to failure of AVF maturation. We hypothesized that early AVF maturation is associated with generation of reactive oxygen species and activation of the HIF-1 pathway, potentially promoting neointimal hyperplasia. We tested this hypothesis using a previously reported mouse AVF model that recapitulates human AVF maturation.

Methods—Aortocaval fistulae were created in C57Bl/6 mice, and compared to sham-operated mice. AVFs or inferior vena cavas were analysed using a microarray, Amplex Red for extracellular H_2O_2, qPCR, immunohistochemistry, and immunoblotting for HIF-1α, and immunofluorescence for NOX-2, nitrotyrosine, HO-1 and VEGF-A.

[§]Correspondence: Dr Nirvana Sadaghianloo, Service de Chirurgie Vasculaire, Centre Hospitalier Universitaire de Nice, Hôpital Pasteur 1, 30 Voie Romaine, 06000 Nice. sadaghianloo.n@chu-nice.fr.

Authors' contributions

NS, KY, HB, MT, MH and CP carried out the experiments, performed the statistical analysis, and drafted the paper. SD, RH and JM participated in the design of the study. AD conceived of the study, and participated in its design and coordination, interpreted the data, and edited the manuscript. All authors read and approved the final manuscript.

Results—Oxidative stress was higher in AVF compared to control veins, with more H_2O_2 (p=0.007) and enhanced nitrotyrosine immunostaining (p=0.005). Immunohistochemistry and immunoblot showed increased HIF-1α immunoreactivity in the AVF endothelium; HIF-1 targets NOX-2, HO-1 and VEGF-A were overexpressed in the AVF (p<0.01). AVF expressed increased numbers of HIF-1α (p<0.0001) and HO-1 (p<0.0001) mRNA transcripts.

Conclusions—Oxidative stress increases in mouse AVF during early maturation, with increased expression of HIF-1α and its target genes NOX-2, HO-1 and VEGF-A. These results suggest that clinical strategies to improve AVF maturation could target the HIF-1 pathway.

Keywords

Arteriovenous fistula; Vein; Vascular endothelium; Hypoxia; HIF-1; VEGF; HO-1; NADPH oxydase

1. Background

Although arteriovenous fistulae (AVF) are the preferred vascular access for hemodialysis for patients with end-stage renal disease, the functional results are not optimal, with one-year patency frequently reported in the range of 60–65%.[1–3] AVF maturation is complex and requires cellular migration and proliferation, as well as extracellular matrix deposition and remodeling to achieve outward remodelling and wall thickening.[4, 5] Both outward remodeling, e.g. increased diameter, and wall thickening are needed for the vein to adapt to the arterial environment, where hemodynamic conditions are different and oxygen tension is increased. The forces that control venous adaptation to the arterial environment are not well understood, as insufficient diameter expansion can lead to failure of AVF maturation whereas excessive wall thickening can lead to the development of juxta-anastomotic stenosis, both of which prevent clinical use of the fistula.

Molecular mechanisms of venous remodeling remain poorly understood, but include: endothelial signaling via eNOS and endothelin-1 signaling[6–9], inflammatory and coagulation pathways via IL-6, IL-8, TNF-α, and IL-10[7, 8], extracellular matrix regulators including MMP-2, MMP-9, TIMP, and ADAMTS-1[10–12], and growth factors and cell adhesion molecules such as IGF-1, PDGF, VEGF, selectin, and VCAM-1[7, 13–15].

Although much research focuses on the mediators that control the response to arterial hemodynamic forces, another mechanism important during AVF maturation may involve the response of the vein to the altered oxygenation of the arterial environment. Hypoxia-inducible factor-1 (HIF-1) is a key transcription factor that regulates the cellular response to oxygen and hypoxic injury.[16] HIF-1 can also be stabilized in normoxic conditions as a consequence of cell injury and oxidative stress.[17] Oxidative stress have been shown to be present in the vein-graft anastomosis,[18] and therefore can play a similar role in increasing HIF-1 expression during AVF maturation. Downstream mechanisms of the HIF-1 pathway include activation of the VEGF pathway, which promotes angiogenesis and arteriogenesis, and regulates vascular tone, via heme oxygenase-1 (HO-1), all of which can stimulate neointimal hyperplasia.[13] Therefore, HIF-1 is an attractive therapeutic target for vascular therapy using pharmacologic agents or gene therapy.[19, 20]

The aim of the present study was to determine if expression of HIF-1 and its downstream targets increases during early AVF maturation, using a mouse model of AVF maturation that recapitulates human AVF maturation.[21] We hypothesized that HIF-1 expression increases during AVF maturation, and therefore this pathway might be a candidate for translational therapy to improve AVF maturation.

2. Methods

2.1. Experimental animals

All animal experiments were performed in compliance with federal guidelines and with approval from the Institutional Animal Care and Use Committee of Yale University. The appropriate anesthesia and analgesia were given as described in our previous studies.[21, 22] Male C57/BL6 mice (body weight: 20–30 g) were used for this study. Briefly, 4% isoflurane in 0.8 l/min O2 was delivered via an isoflurane vaporizer for induction and decreased to 2–3% after mice were anesthesized. Under general anesthesia, a midline laparotomy was made, and the aorta and inferior vena cava (IVC) were exposed. The proximal infrarenal aorta and distal aorta were dissected for clamp placement and needle puncture, respectively; the vena cava was not dissected free from the aorta. After the aorta was clamped just below the left renal artery, a 25-gauge needle was used to puncture the aorta through into the IVC. The surrounding connective tissue was used for hemostatic compression. No heparin was used during the procedure. Successful creation of the AVF was characterized by hemostasis as well as visible pulsatile arterial blood flow in the IVC. Doppler ultrasound was performed both pre- and postoperatively to confirm the presence of the AVF, using the Vevo770 High Resolution Imaging System (VisualSonics) with probe RMV704 (20–60 MHz) under general anesthesia as described above.

2.2. Gene expression microarray analysis

Gene expression in the venous limb of the AVF was compared with that in the IVC of sham mice (day 7; n=4), as described elsewhere.[23] Briefly, RNA was isolated from pooled samples and analyzed for whole genome gene expression using the Mouse Gene 1.0 ST array (Cat. No. 901168; Affymetrix, Santa Clara, California, USA). Significant changes between AVF and sham veins in gene expression were determined using a false discovery rate less than .05 and a fold change of more than 2.0 or less than −2.0. Further experiments were performed regarding HIF-1a and its downstream genes involving angiogenesis and vascular tone regulation.

2.3. Measurement of H_2O_2 production by spectrophotometry

The Amplex Red assay kit (Life Technologies) was used for quantitative, specific, extracellular detection of H_2O_2[24] according to the manufacturer's protocol.[25–27] Briefly, prior to euthanasia, mice were infused with a modified Krebs-Ringer solution containing 145 mM NaCl, 5.7 mM sodium phosphate, 4.86 mM KCl, 0.54 mM CaCl2, 1.22 mM MgSO4, 5.5 mM glucose, at pH 7.4 and 4°C. The venous limb of AVF mice or controls were then excised, and adherent fat or thombi were removed. Vessels were cut in 2 mm rings and transferred to a 96-well plates where they were incubated with Amplex Red (10-acetyl-3,7-dihydroxyphenoxazine) (50μM) and horseradish peroxidase (0.1 U/ml), for 1h at 37°C and

protected from light. H_2O_2 standards (0–0.125 μM) were used as control. A spectrophotometer was used to measure absorbance at 560 nm. Background absorbance, measured in a control reaction without H_2O_2 or sample, was subtracted, and H_2O_2 accumulation was normalized for dry tissue weight (picomoles per milligram of dry tissue).

2.4. RNA extraction and quantitative PCR analysis

The venous limb of the AVF or the control IVC were harvested under general anesthesia just before euthanasia. Expression for the gene of interest was determined using quantitative real-time PCR. Total RNA from the vessels was isolated using the RNeasy Mini kit with digested DNase I (Qiagen). RNA quality was confirmed by the 260-to-280-nm ratio. The SuperScript III First-Strand Synthesis Supermix (Invitrogen) was used for reverse transcription. SYBR Green Supermix (Bio-Rad Laboratories) was used for real-time quantitative PCR, with a 35-cycles amplification using the iQ5 Real-Time PCR Detection System (Bio-Rad Laboratories). Primer efficiencies were determined by melt curve analysis. All samples were normalized by amplification of a housekeeping gene RNA. Primers sequences are listed in Table 1.

2.5. SDS-PAGE and Western Blot analysis

Explanted venous limbs of AVFs and controls were snap frozen in liquid nitrogen and stored at −80° until further process. Protein samples were obtained by mechanical grinding of each vessel in ice-cold lysis buffer (50uM Tris-HCl, 1% NP-40, 0.1% SDS, 0.1% deoxycholic acid, 0.1mM EDTA, 0.1 mM EGTA, protease and phosphatase inhibitors). Protein concentration was determined by spectrophotometry (DC Protein assay, Bio-Rad Laboratories). Equal amounts of protein for each group were then loaded for SDS-page, transfered on polyvinylidene difluoride membranes, and followed by Western Blot analysis. The membranes were incubated overnight at 4°C with one of the following primary antibody : anti-β-Actin (Sigma Aldrich) 1:5000 and anti-HIF-1α (Novus Biologicals) 1:2000. Secondary antibodies were HRP-linked. Signals were detected using the ECL detection reagent (Life Technologies).

2.6. Immunohistochemistry

At euthanasia, en bloc extraction of the AVF or the infrarenal aorta + IVC (control) was performed after perfusion-fixation with PBS followed by 10% formalin. The tissue block was then embedded in paraffin and cut into 5μm cross-sections. Immunohistochemistry was performed using the Dako EnVision+ Dual Link System-HRP (Dako, Carpinteria, CA). Sections were heated in citric acid buffer (pH 6.0) at 100°C for 10 min using the Lab Vision PT Module (Thermo Scientific, Kalamazoo, MI) for antigen retrieval, then treated with 0.3% hydrogen peroxide in methanol for 30 min at room temperature to block endogenous peroxidase activity. They were incubated with 5% normal goat serum in PBS (pH 7.4) containing 0.05% Triton X-100 for 1 h at room temperature to block nonspecific protein-binding sites. Sections were then incubated at 4°C with the anti-HIF-1α primary antibody diluted at 1:50 in PBS containing 0.05% Triton X-100. After an overnight incubation, sections were incubated with EnVision reagents for 1 h at room temperature and treated with the Dako Liquid DAB+ Substrate Chromogen System (Dako) to visualize the reaction

products. Finally, sections were counterstained with Dako Mayer's Hematoxylin (Lillie's Modification) Histological Staining Reagent (Dako).

2.7. Immunofluorescence

Tissue extraction procedure was the same as above. Sections were deparaffined and blocked with 5% bovine serum albumine before incubation with antibodies directed against HO-1 (ab13243, Abcam, Cambridge, MA), Nitrotyrosin (ab7048), NOX-2 (ab31092), VEGFA (ab51745), and vWF (ab11713) overnight at 4°C. Secondary antibodies were linked to Alexa Fluor 488 and 568 (Invitrogen, Carlsbad, CA). Sections were stained with 4,'6-diamidino-2-phelylindole (DAPI, Invitrogen) to mark nuclei. Nitrotyrosine satining density was reported as density per area. Positively staining cells for NOX-2 and HO-1were counted in five high-power fields.

2.8. Statistical analysis

Statistical analysis was performed using GraphPad Prism (version 6) software. All data are means ± SD. Unpaired Student's *t* test was performed after spectrophotometry, densitometry, and cell count analysis. One-way ANOVA and post-hoc analysis were performed for the qPCR experiment. Densitometry analysis after Western Blot was performed on scanned images using Quantity One software (Bio-Rad). After adjustment to multiple comparisons, P values less than 0.05 were considered significant.

3. Results

We previously reported that the mouse aortocaval AVF model recapitulates human AVF maturation.[21] Using this model, we also previously reported a microarray analysis (day 7) with direct qPCR validation showing distinct temporal patterns of expression of several ECM components, suggesting a highly regulated response to injury during early AVF maturation.[23] Interestingly, the microarray analysis showed downregulation of 27 of the 83 genes involved in the oxidative phosphorylation pathway, downregulation of 12 of the 18 genes involved in mitochondrial long chain fatty acid beta-oxidation, and 10 of the 13 genes involved in mitochondrial unsaturated fatty acid beta-oxidation (Table 2), suggesting the presence of oxidative stress during early AVF maturation.

To determine if oxidative stress is present during early AVF maturation, explanted AVF and control veins (day 3) were incubated in Amplex Red reagent to directly measure H_2O_2 excretion; spectrophotometry showed that extracellular H_2O_2 was significantly higher in AVF compared to control veins (Figure 1). To confirm increased oxidative stress during AVF maturation, immunofluorescence staining of the AVF showed increased nitrotyrosine at both days 3 and 7 compared to control veins (Figure 2A, 2B). Interestingly, nitrotyrosine was increased in both the endothelium as well as the media of the AVF, suggesting colocalization of oxidative stress with the site of future development of neointimal hyperplasia (Figure 2A). These results suggest that the oxidative stress pathway is active during early AVF maturation.

Since oxidative stress is present during AVF maturation, we determined if HIF-1α and its targets NOX-2, HO-1, and VEGF-A are expressed during early AVF maturation.

Immunofluorescence staining of the AVF showed increased immunoreactivity of NOX-2, HO-1, and VEGF-A at both days 3 and 7 compared to control veins (Figure 2A, 2C–E). Similar to the distribution of nitrotyrosine, NOX-2, HO-1, and VEGF-A immunoreactivity was present throughout the AVF (Figure 2A). Similarly, HIF-1α protein expression was increased in AVF compared to control veins, using both Western blot as well as immunohistochemistry that showed the enothelial location of HIF-1α in the AVF (Figure 3).

Since protein expression of HIF-1α, as well as its targets NOX-2, HO-1, and VEGF-A, are increased during early AVF maturation, we examined the RNA expression of these components of the oxidative stress pathway. Microarray analysis (day 7) suggested sustained increased RNA expression of HIF-1α, NOX-2, and HO-1, but not VEGF-A (Table 3). qPCR confirmed elevated expression of HIF-1α and HO-1, but not VEGF-A (Figure 4); NOX-2 expression could not be determined (data not shown). These results suggest complex patterns of expression regulating the oxidative stress pathway during AVF maturation (Figure 5), e.g. oxidative stress is present and HIF-1α expression is increased during AVF maturation.

4. Discussion

In a mouse AVF model that recapitulates human AVF maturation, oxidative stress is present during early venous adaptation to the arterial environment (days 3 and 7; Figures 1 and 2). Expression of both HIF-1α, as well as its downstream targets NOX-2 and HO-1, were increased in the AVF compared to control veins (Figures 3 and 4). These results colocalize the presence of HIF-1 with oxidative stress during early AVF maturation, suggesting a potential target to enhance early venous adaptation to the arterial environment.

Oxidative stress is associated with end-stage renal disease and stimulates synthesis and secretion of reactive oxygen species (ROS).[28–30] Several studies have shown increased oxidative stress and superoxide anions in the neointimal hyperplasia lesions of AVF.[18, 31] ROS are known to regulate diverse processes during venous adaptation, including smooth muscle cell migration and proliferation and activation of latent MMP,[32–34] similar to the function of MMP during development of venous pathology.[35] ROS and particularly hydrogen peroxide also play a significant role in the hypoxia pathway by activating HIF-1α, via the activation of the NADPH oxydase.[36] We showed increased excreted hydrogen peroxide, nitrotyrosine staining, and NOX-2 staining in the venous limb of the AVF during early maturation (Figures 1 and 2), confirming the presence of oxidative stress during AVF maturation.

HIF-1 is a transcription factor that consists of two sub-units. During normoxic conditions, the HIF-1α subunit is degraded in the cytosol, whereas the HIF-1β subunit is consitutively present in the nucleus. However, during hypoxic conditions there is inhibited degradation of the HIF-1α subunit, which then enters the nucleus to binds to the HIF-1β and other cofactors, activating the hypoxia response element (HRE) of some gene promoters to stimulate this pathway functions.[16] We show that increased expression of HIF-1α also occurs early during AVF maturation, which is localized to the venous endothelium (Figure 3B). These data suggests that AVF creation may induce either hypoxic or oxidative injury in

the fistula endothelium, consistent with other models of intimal hyperplasia following endothelial injury.[37, 38]

Hypoxia is suspected of playing a role in the pathogenesis of various diseases of the vascular wall. HIF pathway activation has been studied in the pathophysiology of both atherosclerosis (including foam cell formation, cellular proliferation, plaque ulceration, hemorrhage and rupture) and arterial aneurysms (including weakening, dilation and rupture of the arterial wall).[19] Misra et al. showed increased HIF-1α expression and other hypoxia-related proteins in a mouse-model of failing AVF with renal insufficiency.[12] Our data shows HIF-1α expression during normal AVF maturation, suggesting that this transcription factor is not necessarily deleterious. However, it is unclear whether this increase is mechanistic or a secondary phenomenon during AVF maturation and/or failure, and whether its role evolves in time. Therefore, it is not clear whether this pathway should be up- or down-regulated.[19] Similarly, it is not surprising that changes in mRNA expression of numerous proteins involved in metabolism and mitochondrial ROS production occur during AVF maturation (Table 2); however, these data are consistent with downregulation of the oxidative phosphorylation pathways of metabolism, suggesting that energy production during AVF maturation may be via alternative anaerobic metabolic pathways, such as the glycolytic, pentose phosphate, or glutamine pathways.

5. Conclusions

In a mouse model of AVF maturation, AVF creation was rapidly followed by increased release of ROS and increased HIF-1α protein expression. NOX-2, HO-1 and VEGF-A, target proteins induced by HIF-1, were also highly expressed. This data suggests that AVF creation induces hypoxic injury in the wall of the fistula, and triggers the HIF-1 pathway. Therefore, early manipulation of the HIF-1 pathway is a potential therapeutic target to enhance AVF maturation.

Acknowledgments

The authors thank Drs Taylor Williams, Roland Assi, Daniel Lu, Daniel Wong and Guangxin Li for their contributions to the study design.

Funding: The project described was supported by the Award Number R01-HL095498 (AD) and the PO1-NS-062686 (JM) from the NIH, the Ohse award from Yale Department of Surgery (KY, CP) and the Uehara Memorial Foundation (KY, MT). Time spent in the Dardik laboratory by NS was sponsored by University of Nice-Sophia Antipolis research grant, the French Society for Vascular Surgery (SCV) subsistence grant, and Abbott Vascular young researcher grant.

References

1. Tordoir JHM, Rooyens P, Dammers R, van der Sande FM, de Haan M, Yo TI. Prospective evaluation of failure modes in autogenous radiocephalic wrist access for haemodialysis. Nephrol Dial Transplant. 2003; 18:378–383. [PubMed: 12543895]
2. Roy-Chaudhury P, Spergel LM, Besarab A, Asif A, Ravani P. Biology of arteriovenous fistula failure. J Nephrol. 2007; 20:150–163. [PubMed: 17514619]
3. Rooijens PP, Tordoir JH, Stijnen T, Burgmans JP, Smet de AA, Yo TI. Radiocephalic wrist arteriovenous fistula for hemodialysis: Meta-analysis indicates a high primary failure rate. Eur J Vasc Endovasc Surg. 2004; 28:583–589. [PubMed: 15531191]

4. Rothuizen TC, Wong C, Quax PH, van Zonneveld AJ, Rabelink TJ, Rotmans JI. Arteriovenous access failure: More than just intimal hyperplasia? Nephrol Dial Transplant. 2013; 28:1085–1092. [PubMed: 23543595]

5. Lu DY, Chen EY, Wong DJ, Yamamoto K, Protack CD, Williams WT, Assi R, Hall MR, Sadaghianloo N, Dardik A. Vein graft adaptation and fistula maturation in the arterial environment. J Surg Res. 2014; 188:162–173. [PubMed: 24582063]

6. Caplice NM, Wang S, Tracz M, Croatt AJ, Grande JP, Katusic ZS, Nath KA. Neoangiogenesis and the presence of progenitor cells in the venous limb of an arteriovenous fistula in the rat. Am J Physiol Renal Physiol. 2007; 293:F470–F475. [PubMed: 17344190]

7. Croatt AJ, Grande JP, Hernandez MC, Ackerman AW, Katusic ZS, Nath KA. Characterization of a model of an arteriovenous fistula in the rat: The effect of l-name. Am J Pathol. 2010; 176:2530–2541. [PubMed: 20363917]

8. Nath KA, Kanakiriya SK, Grande JP, Croatt AJ, Katusic ZS. Increased venous proinflammatory gene expression and intimal hyperplasia in an aorto-caval fistula model in the rat. Am J Pathol. 2003; 162:2079–2090. [PubMed: 12759262]

9. Jones GT, van Rij AM, Packer SG, Walker RJ, Stehbens WE. Venous endothelial changes in therapeutic arteriovenous fistulae. Atherosclerosis. 1998; 137:149–156. [PubMed: 9568747]

10. Lee ES, Shen Q, Pitts RL, Guo M, Wu MH, Sun SC, Yuan SY. Serum metalloproteinases mmp-2, mmp-9, and metalloproteinase tissue inhibitors in patients are associated with arteriovenous fistula maturation. J Vasc Surg. 2011; 54:454–459. discussion 459–460. [PubMed: 21620625]

11. Misra S, Lee N, Fu AA, Raghavakaimal S, Mandrekar J, Bjarnason H, McKusick MA, Iruela-Arispe L, Mukhopadhyay D. Increased expression of a disintegrin and metalloproteinase thrombospondin 1 in thrombosed hemodialysis grafts. J Vasc Interv Radiol. 2008; 19:111–119. [PubMed: 18192475]

12. Misra S, Shergill U, Yang B, Janardhanan R, Misra KD. Increased expression of hif-1alpha, vegf-a and its receptors, mmp-2, timp-1, and adamts-1 at the venous stenosis of arteriovenous fistula in a mouse model with renal insufficiency. J Vasc Interv Radiol. 2010; 21:1255–1261. [PubMed: 20598569]

13. Juncos JP, Tracz MJ, Croatt AJ, Grande JP, Ackerman AW, Katusic ZS, Nath KA. Genetic deficiency of heme oxygenase-1 impairs functionality and form of an arteriovenous fistula in the mouse. Kidney Int. 2008; 74:47–51. [PubMed: 18368029]

14. Yang B, Janardhanan R, Vohra P, Greene EL, Bhattacharya S, Withers S, Roy B, Nieves Torres EC, Mandrekar J, Leof EB, Mukhopadhyay D, Misra S. Adventitial transduction of lentivirus-shrna-vegf-a in arteriovenous fistula reduces venous stenosis formation. Kidney Int. 2014; 85:289–306. [PubMed: 23924957]

15. Chang C-J, Ko Y-S, Ko P-J, Hsu L-A, Chen C-F, Yang C-W, Hsu T-S, Pang J-HS. Thrombosed arteriovenous fistula for hemodialysis access is characterized by a marked inflammatory activity. Kidney Int. 2005; 68:1312–1319. [PubMed: 16105066]

16. Mazure NM, Brahimi-Horn MC, Berta MA, Benizri E, Bilton RL, Dayan F, Ginouvès A, Berra E, Pouysségur J. Hif-1: Master and commander of the hypoxic world. A pharmacological approach to its regulation by siRNAs. Biochem Pharmacol. 2004; 68:971–980. [PubMed: 15313390]

17. Pouysségur J, Mechta-Grigoriou F. Redox regulation of the hypoxia-inducible factor. Biol Chem. 2006; 387:1337–1346. [PubMed: 17081104]

18. Weiss MF, Scivittaro V, Anderson JM. Oxidative stress and increased expression of growth factors in lesions of failed hemodialysis access. Am J Kidney Dis. 2001; 37:970–980. [PubMed: 11325679]

19. Lim CS, Kiriakidis S, Sandison A, Paleolog EM, Davies AH. Hypoxia-inducible factor pathway and diseases of the vascular wall. J Vasc Surg. 2013; 58:219–230. [PubMed: 23643279]

20. Beuck S, Schänzer W, Thevis M. Hypoxia-inducible factor stabilizers and other small-molecule erythropoiesis-stimulating agents in current and preventive doping analysis. Drug Test Anal. 2012; 4:830–845. [PubMed: 22362605]

21. Yamamoto K, Protack CD, Tsuneki M, Hall MR, Wong DJ, Lu DY, Assi R, Williams WT, Sadaghianloo N, Bai H, Miyata T, Madri JA, Dardik A. The mouse aortocaval fistula recapitulates

human arteriovenous fistula maturation. Am J Physiol Heart Circ Physiol. 2013; 305:H1718–H1725. [PubMed: 24097429]

22. Yamamoto K, Li X, Shu C, Miyata T, Dardik A. Technical aspects of the mouse aortocaval fistula. J Vis Exp. 2013:e50449. [PubMed: 23892387]
23. Hall MR, Yamamoto K, Protack CD, Tsuneki M, Kuwahara G, Assi R, Brownson KE, Bai H, Madri JA, Dardik A. Temporal regulation of venous extracellular matrix components during arteriovenous fistula maturation. J Vasc Access. 2015; 16:93–106. [PubMed: 25262757]
24. Cai, H., Dikalov, S., Griendling, KK., Harrison, DG. Vascular biology protocols. Vol. 139. Springer; 2007. Detection of reactive oxygen species and nitric oxide in vascular cells and tissues: Comparison of sensitivity and specificity.
25. Weber DS, Rocic P, Mellis AM, Laude K, Lyle AN, Harrison DG, Griendling KK. Angiotensin II-induced hypertrophy is potentiated in mice overexpressing p22phox in vascular smooth muscle. Am J Physiol Heart Circ Physiol. 2005; 288:H37–H42. [PubMed: 15345488]
26. Miller AA, Maxwell KF, Chrissobolis S, Bullen ML, Ku JM, Michael De Silva T, Selemidis S, Hooker EU, Drummond GR, Sobey CG, Kemp-Harper BK. Nitroxyl (hno) suppresses vascular nox2 oxidase activity. Free Radic Biol Med. 2013; 60:264–271. [PubMed: 23459072]
27. Miller AA, Drummond GR, De Silva TM, Mast AE, Hickey H, Williams JP, Broughton BR, Sobey CG. Nadph oxidase activity is higher in cerebral versus systemic arteries of four animal species: Role of nox2. Am J Physiol Heart Circ Physiol. 2009; 296:H220–H225. [PubMed: 19028794]
28. Loughrey CM, Young IS, Lightbody JH, McMaster D, McNamee PT, Trimble ER. Oxidative stress in haemodialysis. QJM. 1994; 87:679–683. [PubMed: 7820542]
29. Witko-Sarsat V, Friedlander M, Capeillère-Blandin C, Nguyen-Khoa T, Nguyen AT, Zingraff J, Jungers P, Descamps-Latscha B. Advanced oxidation protein products as a novel marker of oxidative stress in uremia. Kidney Int. 1996; 49:1304–1313. [PubMed: 8731095]
30. Spittle MA, Hoenich NA, Handelman GJ, Adhikarla R, Homel P, Levin NW. Oxidative stress and inflammation in hemodialysis patients. Am J Kidney Dis. 2001; 38:1408–1413. [PubMed: 11728983]
31. Tsapenko MV, d'Uscio LV, Grande JP, Croatt AJ, Hernandez MC, Ackerman AW, Katusic ZS, Nath KA. Increased production of superoxide anion contributes to dysfunction of the arteriovenous fistula. Am J Physiol Renal Physiol. 2012; 303:F1601–F1607. [PubMed: 22993073]
32. Satoh K, Nigro P, Berk BC. Oxidative stress and vascular smooth muscle cell growth: A mechanistic linkage by cyclophilin a. Antioxid Redox Signal. 2010; 12:675–682. [PubMed: 19747062]
33. Rao GN, Berk BC. Active oxygen species stimulate vascular smooth muscle cell growth and proto-oncogene expression. Circ Res. 1992; 70:593–599. [PubMed: 1371430]
34. Castier Y, Brandes RP, Leseche G, Tedgui A, Lehoux S. P47phox-dependent nadph oxidase regulates flow-induced vascular remodeling. Circ Res. 2005; 97:533–540. [PubMed: 16109921]
35. Goyal P, Weissmann N, Grimminger F, Hegel C, Bader L, Rose F, Fink L, Ghofrani HA, Schermuly RT, Schmidt HH, Seeger W, Hänze J. Upregulation of nad(p)h oxidase 1 in hypoxia activates hypoxia-inducible factor 1 via increase in reactive oxygen species. Free Radic Biol Med. 2004; 36:1279–1288. [PubMed: 15110393]
36. Roque M, Fallon JT, Badimon JJ, Zhang WX, Taubman MB, Reis ED. Mouse model of femoral artery denudation injury associated with the rapid accumulation of adhesion molecules on the luminal surface and recruitment of neutrophils. Arterioscler Thromb Vasc Biol. 2000; 20:335–342. [PubMed: 10669628]
37. Hancock WW, Adams DH, Wyner LR, Sayegh MH, Karnovsky MJ. Cd4+ mononuclear cells induce cytokine expression, vascular smooth muscle cell proliferation, and arterial occlusion after endothelial injury. Am J Pathol. 1994; 145:1008–1014. [PubMed: 7977633]

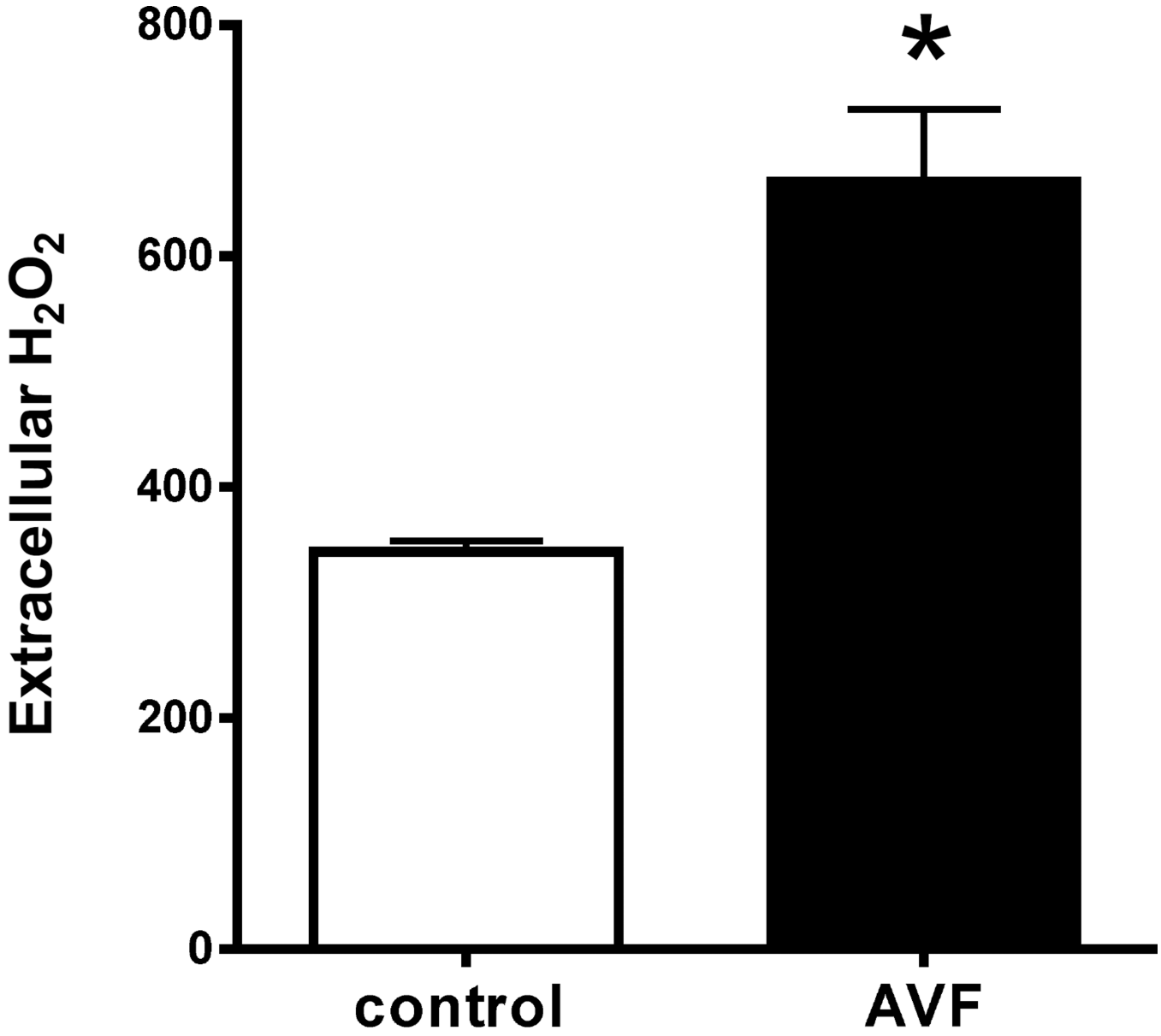

Figure 1.

Extracellular H_2O_2 during AVF maturation (day 3). Bar graph shows spectrophotometry-measured absorbance (560 nm) to quantify the amount of H_2O_2 excreted by the tissue (picomoles per milligram of dry tissue). *, p=0.007; n=3.

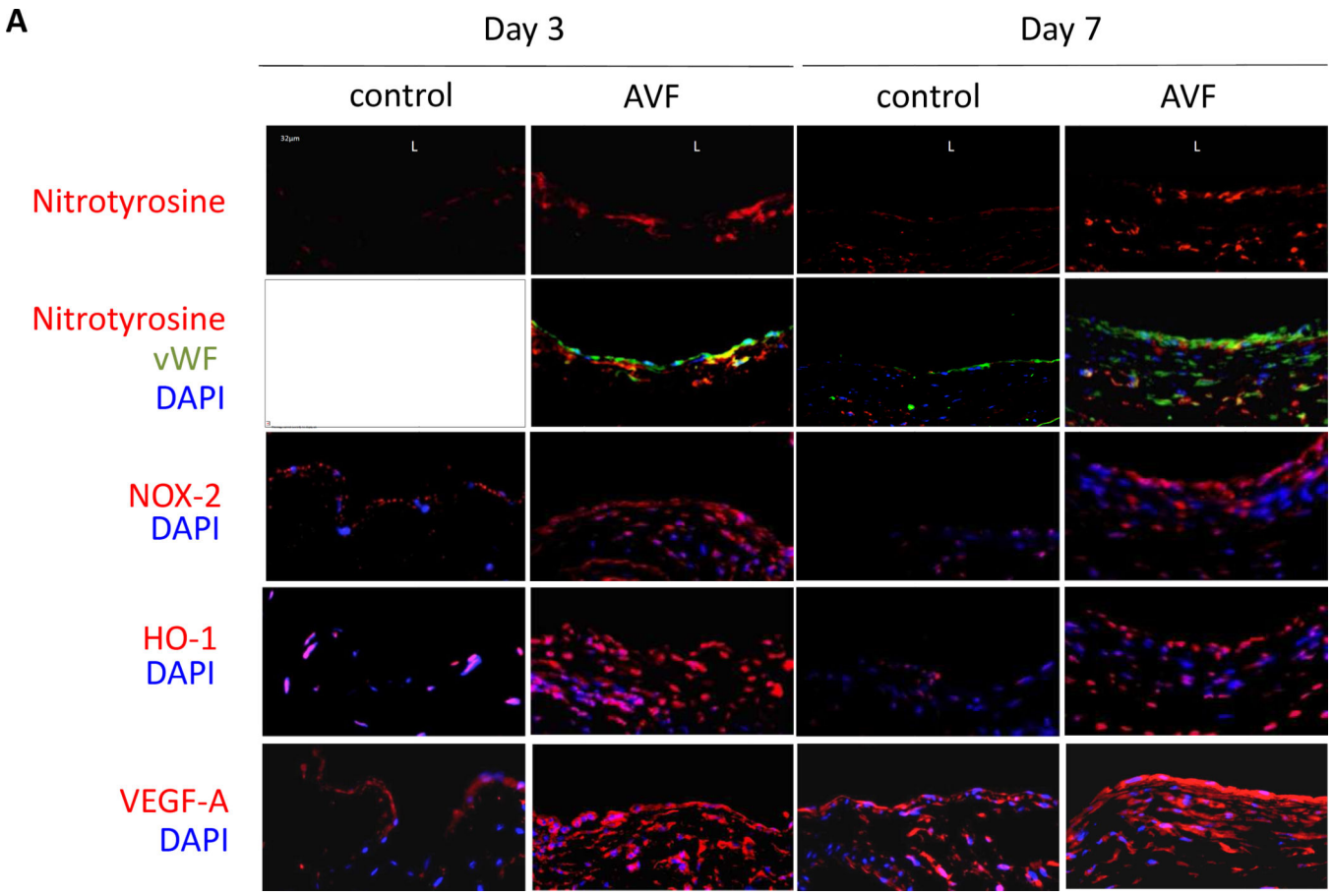

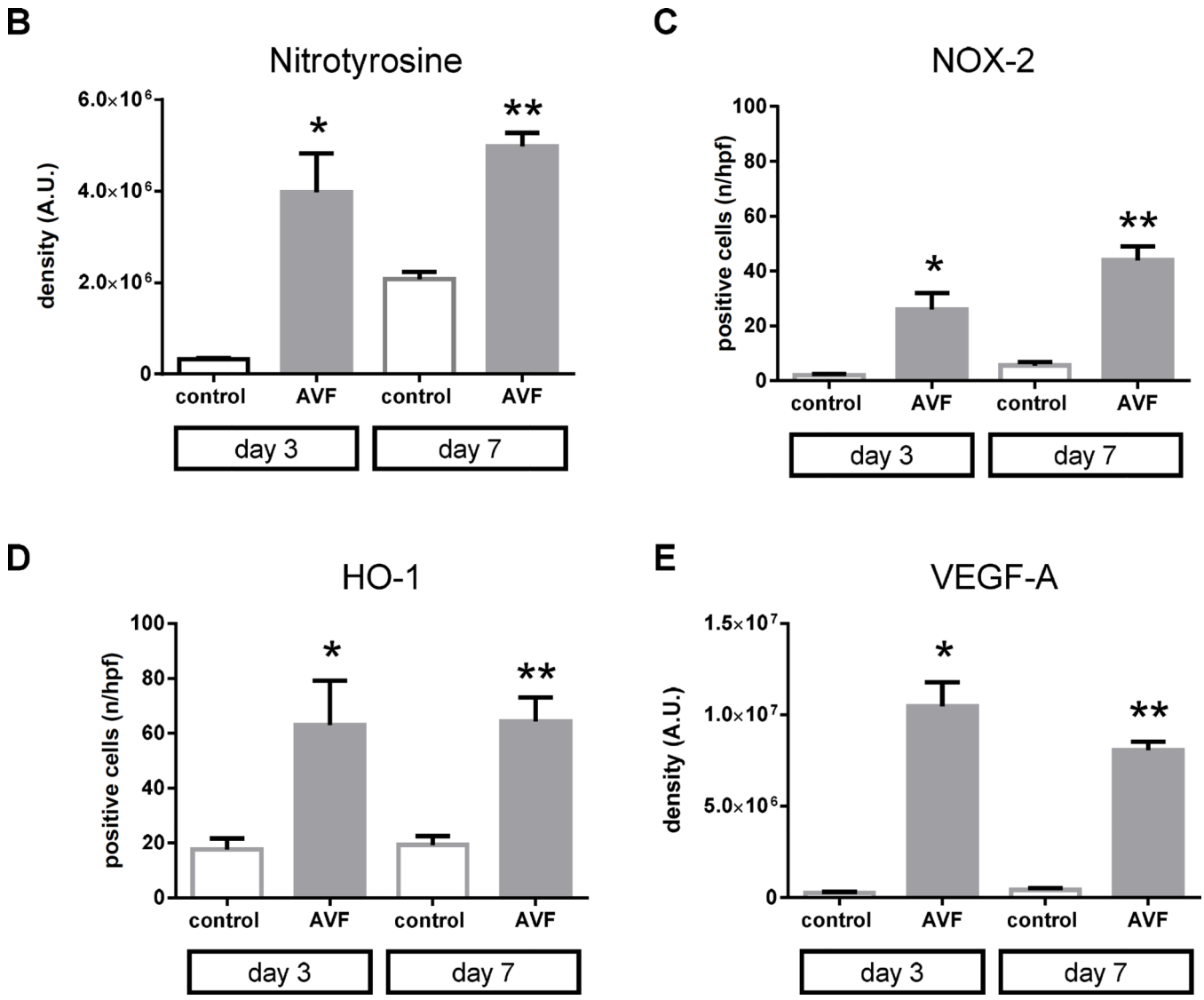

Figure 2.

Oxidative stress pathway during AVF maturation. **A)** Representative immunofluorescence showing nitrotyrosine (upper 2 rows), NOX-2 (third row), HO-1 (fourth row) and VEGF-A (bottom row) in sham vein and AVF, matched at postoperative days 3 and 7. L, Luminal side of the vein. Scale bar, 32μm; magnification, ×40. **B)** Bar graph shows quantification of nitrotyrosine immunofluorescence intensity. *, p = 0.0123; **, p = 0.001. n=3. **C)** Bar graph shows number of cells positive for NOX-2. *, p = 0.0166; **, p = 0.0018. n=3. **D)** Bar graph shows number of cells positive for HO-1. *, p = 0.0091; **, p = 0.0011. n=3. **E)** Bar graph shows quantification of VEGF-A immunofluorescence intensity. *, p = 0.0015; **, p < 0.0001. n=3. A.U., arbitrary units.

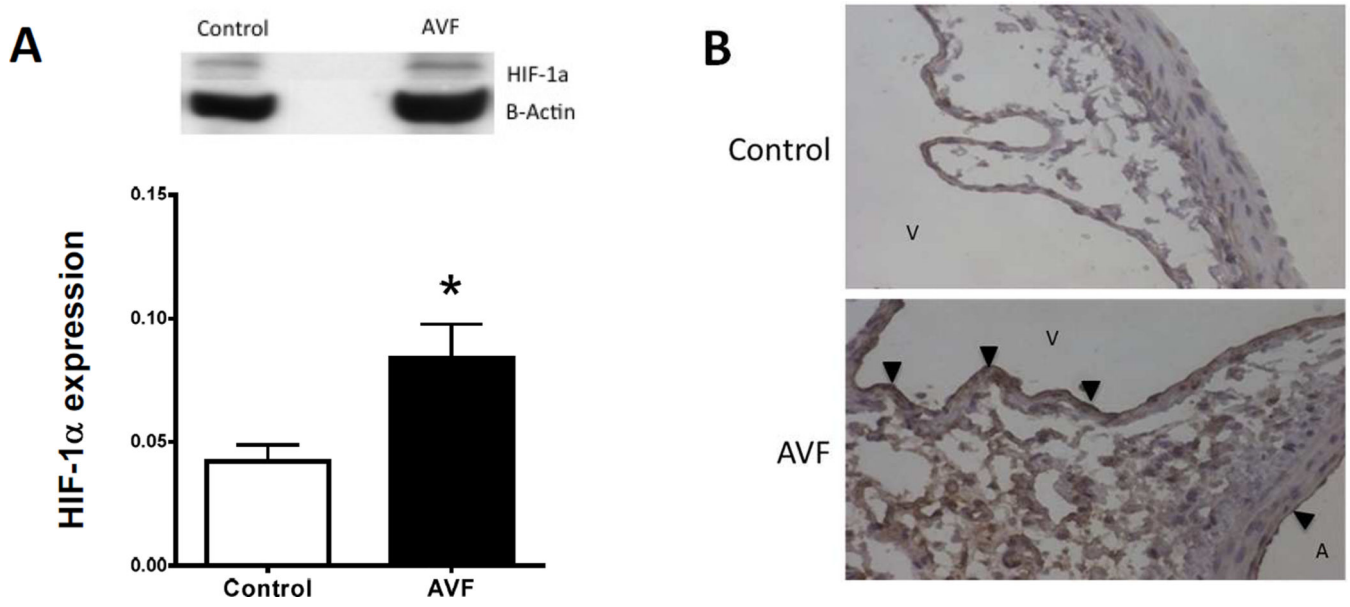

Figure 3.

HIF-1α protein expression during AVF maturation (day 3). **A)** Representative Western blot and bar graph showing increased HIF-1α expression in the AVF compared to control vein. n=3. *, p=0.0499. **B)** Photomicrographs show representative immunohistochemistry for HIF-1α protein; upper panel, control vein; lower panel, AVF. A, aorta; V, vein (inferior vena cava); black arrowheads show HIF-1α expression in the AVF venous and arterial endothelium. n=3.

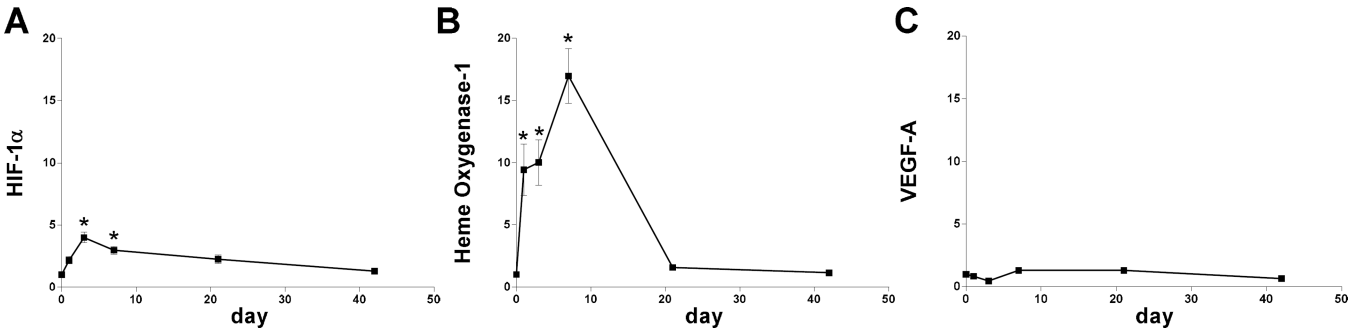

Figure 4.

RNA expression during AVF maturation. **A)** Bar graph shows RNA expression of HIF-1α during AVF maturation relative to sham veins, normalized to day 0 expression; $p < 0.0001$; n=5–8. *, $p < 0.0001$ (day 3); *, $p = 0.0015$ (day 7). **B)** Bar graph shows RNA expression of HO-1 during AVF maturation relative to sham veins, normalized to day 0 expression; $p < 0.0001$; n=5–8. *, $p = 0.0063$ (day 1); *, $p = 0.0033$ (day 3); *, $p < 0.0001$ (day 7). **C)** Bar graph shows RNA expression of VEGF-A during AVF maturation relative to sham veins, normalized to day 0 expression; $p = 0.0001$; n=5–8.

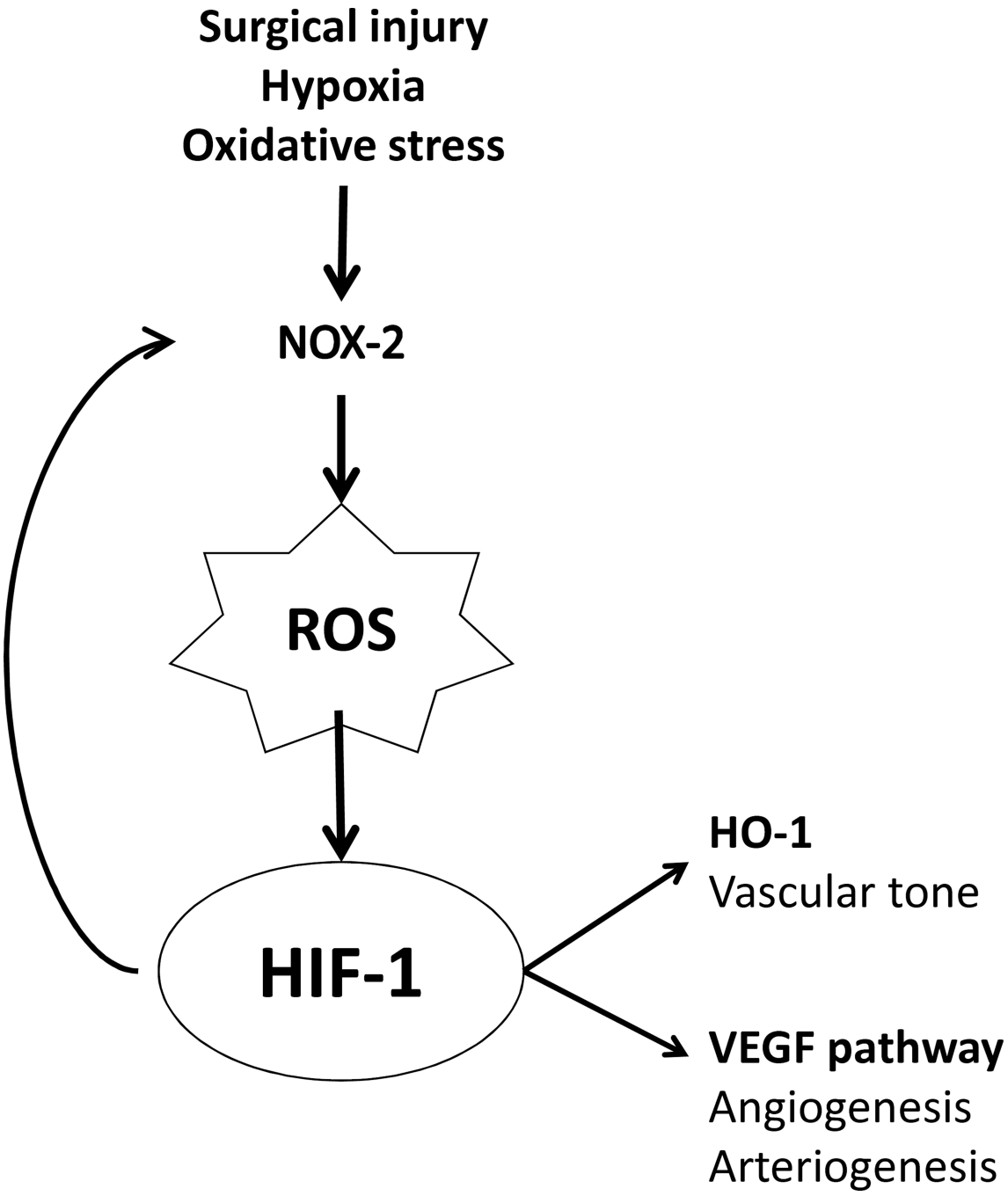

Figure 5.

Oxidative stress pathway during AVF maturation. Surgical creation of an AVF provokes vessel injury with activation of NOX-2, generating reactive oxygen species that stabilizes HIF-1α and generates positive feedback to upregulate NOX-2 expression. HIF-1α also stimulates downstream pathways including HO-1, a regulator of vascular tone, and VEGF-A, a promoter of angiogenesis and arteriogenesis.

Table 1

qPCR primer sequences

Gene name	Gene symbol	Primers		Product size (bp)
HIF-1α	Hif1a	Sense	GATGACGGCGACATGGTTTA	290
		Antisense	CTCACTGGGCCATTTCTGTG	
HO-1	HMOX1	Sense	ACCTTCCCGAACA TCGACAG	157
		Antisense	TCACCTGCAGCTCCTCAAAC	
VEGF-A	VEGFA	Sense	TGTACCTCCACCATGCCAAG	183
		Antisense	CACAGGACGGCTTGAAGA TG	

Table 2

Significant changes in gene expression during AVF maturation (day 7) compared to the control veins (microarray data): metabolic pathways ($p<0.05$).

Pathway	Gene Symbol	Full name	Fold-change
Oxidative phosphorylation	NDUFV1	NADH dehydrogenase (ubiquinone) flavoprotein 1	−2.9
	CYC1	cytochrome c-1	−2.9
	UQCRFS1	ubiquinol-cytochrome c reductase, Rieske iron-sulfur polypeptide 1	−2.7
	UQCRC1	ubiquinol-cytochrome c reductase core protein 1	−2.7
	NDUFS1	NADH dehydrogenase (ubiquinone) Fe-S protein 1	−2.6
	NDUFB8	NADH dehydrogenase (ubiquinone) 1 beta subcomplex 8	−2.6
	COX Va	cytochrome c oxidase subunit Va	−2.6
	UQCR 10	ubiquinol-cytochrome c reductase, complex III subunit X	−2.5
	NDUFAB1	NADH dehydrogenase (ubiquinone) 1, alpha/beta subcomplex, 1	−2.4
	NDUFA9	NADH dehydrogenase (ubiquinone) 1 alpha subcomplex, 9	−2.4
	NDUFS6	NADH dehydrogenase (ubiquinone) Fe-S protein 6	−2.4
	NDUFA10	NADH dehydrogenase (ubiquinone) 1 alpha subcomplex 10	−2.3
	NDUFS3	NADH dehydrogenase (ubiquinone) Fe-S protein 3	−2.3
	Succinate dehydrogenase		−2.2
	NDUFB6	NADH dehydrogenase (ubiquinone) 1 beta subcomplex, 6	−2.2
	UQCR11	ubiquinol-cytochrome c reductase, complex III subunit XI	−2.2
	NDUFS5	NADH dehydrogenase (ubiquinone) Fe-S protein 5	−2.2
	NDUFS2	NADH dehydrogenase (ubiquinone) Fe-S protein 2	−2.2
	NDUFB9	NADH dehydrogenase (ubiquinone) 1 beta subcomplex, 9	−2.2
	NDUFS8	NADH dehydrogenase (ubiquinone) Fe-S protein 8	−2.1
	ATP5A	ATP synthase, H+ transporting, mitochondrial F1 complex, alpha	−2.1
	NDUFS7	NADH dehydrogenase (ubiquinone) Fe-S protein 7	−2.1
	UQCRH	ubiquinol-cytochrome c reductase hinge protein	−2.1
	NDUFA4	NADH dehydrogenase (ubiquinone) 1 alpha subcomplex, 4	−2.1

Pathway	Gene Symbol	Full name	Fold-change
	Cytochrome C		−2.0
	NDUFB5	NADH dehydrogenase (ubiquinone) 1 beta subcomplex, 5	−2.0
	COX Vb	cytochrome c oxidase subunit Vb	−2.0
Mitochondrial long chain fatty acid beta-oxidation	CPT-1B	carnitine palmitoyltransferase 1b, muscle	−5.9
	ACADVL	acyl-CoA dehydrogenase, very long chain	−4.0
	HADHB	hydroxyacyl-CoA dehydrogenase/3-ketoacyl-CoA thiolase/enoyl-CoA hydratase (trifunctional protein), beta subunit	−3.3
	ACAA2	acetyl-CoA acyltransferase 2	−3.1
	ACSL5	acyl-CoA synthetase long-chain family member 5	−2.8
	Acetyl-CoA acyltransferase		−2.7
	ECHS1	enoyl CoA hydratase, short chain, 1, mitochondrial	−2.7
	HADHA	hydroxyacyl-CoA dehydrogenase/3-ketoacyl-CoA thiolase/enoyl-CoA hydratase (trifunctional protein), alpha subunit	−2.7
	CPT2	carnitine palmitoyltransferase 2	−2.6
	ACADM	acyl-Coenzyme A dehydrogenase, medium chain	−2.4
	HCDH	hydroxyacyl-Coenzyme A dehydrogenase	−2.3
	ACSL1	acyl-CoA synthetase long-chain family member 1	−2.0
Mitochondrial unsaturated fatty acid beta-oxidation	HADHB	hydroxyacyl-CoA dehydrogenase/3-ketoacyl-CoA thiolase/enoyl-CoA hydratase (trifunctional protein), beta subunit	−3.3
	ACAA2	acetyl-CoA acyltransferase 2	−3.0
	ACSL5	acyl-CoA synthetase long-chain family member 5	−2.8
	Acetyl-CoA acyltransferase		−2.7
	HADHA	hydroxyacyl-CoA dehydrogenase/3-ketoacyl-CoA thiolase/enoyl-CoA hydratase (trifunctional protein), alpha subunit	−2.7
	ECHS1	enoyl CoA hydratase, short chain, 1, mitochondrial	−2.7
	DCI	enoyl-CoA delta isomerase 1	−2.5
	ACADM	acyl-Coenzyme A dehydrogenase, medium chain	−2.4
	HCDH	mitochondrial hydroxyacyl-coenzyme a dehydrogenase	−2.3
	ACSL1	acyl-CoA synthetase long-chain family member 1	−2.0

Table 3

Changes in HIF-1 pathway gene expression during AVF maturation (day 7) compared to the control veins (microarray data).

Protein	Gene	Fold change (ratio AVF : Sham)	p-value
NOX-2	CYBB	3.11	0.007
HIF-1α	HIF1a	1.52	0.001
HO-1	Hmox1	3.04	0.0001
VEGF-A	VEGFA	0.48	0.0006